Current-Voltage Characteristics of Platinum Model Electrodes on Yttria-Stabilized Zirconia

Alexander K. Opitz, Michael P. Hörlein, Tobias Huber, Jürgen Fleig

Vienna University of Technology, Institute of Chemical Technologies and Analytics,
Getreidemarkt 9 / 164-EC, 1060 Vienna, Austria
e-mail: alexander.opitz@tuwien.ac.at
phone: 0043-1-58801-15860; fax: 0043-1-58801-15899

Abstract

In this study, the steady state current-overpotential (I-η) characteristics of the oxygen reduction reaction on the system Pt|yttria-stabilized zirconia (YSZ) were investigated at temperatures between 600 and 720 °C. The I-η curve of Pt thin-film model electrodes on YSZ (100) exhibited a quite unexpected behavior, with diffusion limitation at lower and an exponential I-η relationship at high cathodic polarization. This situation was interpreted in terms of two parallel electrochemical oxygen reduction pathways. The diffusion limited path – with an activation energy of the limiting current of 1.57 eV – is attributed to a classical surface path on Pt with diffusion through an impurity phase at the triple phase boundary (TPB) being rate limiting. Stoichiometry polarization is most likely responsible for the exponential part of the I-η curve. In the corresponding second pathway, the oxygen reduction takes place on the YSZ surface with a rate limiting electron supply via the YSZ electrolyte. This interpretation is further supported by good accordance of the obtained activation energy (3.65 eV) with the activation energy of electronic conductivity in YSZ. The data can be used to calculate current contributions in broad temperature and overpotential ranges.

Keywords

oxygen reduction, microelectrodes, triple phase boundary, surface path, reaction pathways

1   Introduction

Platinum electrodes on yttria-stabilized zirconia (YSZ) electrolytes have been employed and investigated from the beginnings of solid state electrochemistry (1) and are still highly important in applications such as gas sensors (2, 3) or micro solid oxide fuel cells (4, 5) as well as in fundamental research (6-14). One basic question deals with the mechanism of the oxygen exchange reaction. Pt on YSZ is generally believed to be a kind of prototype of surface path systems, i.e. systems where all elementary electrode reaction steps proceed on surfaces and the incorporation of oxygen into YSZ takes place at the three phase boundary (TPB) (15, 16). Accordingly, Pt was and is still considered to be an ideal model electrode material for fundamental investigations of oxygen exchange kinetics on solid oxide ion conductors (6, 7, 9-15, 17-54). However, in several recent studies it was called into question that platinum electrodes do behave as ideal as expected from model considerations. Impurities at the TPBs of Pt electrodes were shown to hamper the oxygen exchange reaction (7, 10, 11, 34) and may therefore mask the intrinsic electrochemical behavior of the pure system Pt|YSZ. Also the electrochemical effects of oxygen containing Pt phases (PtO_x) are still under discussion (6, 11, 18, 39, 40). Moreover, in case of polycrystalline thin film model electrodes, an oxygen pathway through the Pt electrode (most likely along Pt grain boundaries) may significantly influence their electrochemical behavior (13, 34, 55-57). All these recent findings show that the mechanism of oxygen exchange on Pt|YSZ is still not that well understood as it is the case in aqueous electrochemistry. Therefore a better understanding of the behavior of this model system can lead to a deeper understanding of electrochemical processes on solid electrolytes.

Impedance spectroscopy (IS) (7, 14, 17, 20, 30, 33, 38, 40, 43, 47, 49-52) and cyclic voltammetry (CV) (6, 11, 17-19, 21, 31-33, 53, 54) have been the most important electrochemical characterization methods used so far in kinetic studies on Pt model electrodes or porous paste electrodes. Steady state dc measurements have also been employed, but less frequently and mostly on porous paste electrodes (30, 35, 44, 45, 48, 52). A possible reason is that steady state current-overpotential (I-η) curves – in contrast to IS and CV – do not include information on the capacitive

behavior. Consequently, separation of different contributions to the polarization is often less straightforward than in impedance spectroscopic studies. On the other hand, steady state I-η measurements offer the advantage of providing information on electrode kinetics also in regimes far from equilibrium conditions with resistive electrode processes not being superimposed by capacitive currents as in CV.

The aim of the present study was the investigation of the current-voltage characteristics of geometrically well-defined, dense Pt (111) microelectrodes on YSZ (100) in the temperature range between 600 and 720 °C. The temperature range was chosen such, that the oxygen exchange mechanism close to equilibrium can safely be assumed to proceed via the surface path with a rate limiting step close to the TPB – as revealed in a previous impedance study (12). From the current-overpotential curves, additional information is obtained on the nature of the rate limiting step close to equilibrium and under low cathodic polarization. Moreover, an additional reaction path is shown to come into play at high cathodic polarization. Consequences of the dc results for the interpretation of impedance measurements are discussed in terms of equivalent circuits.

2 Experimental

2.1 Preparation and characterization of Pt electrodes

Platinum thin film electrodes were prepared by sputter deposition (MED 020 Coating System, BAL-TEC, Germany) of Pt (99.95 % pure, ÖGUSSA, Austria) onto (100)-oriented YSZ single crystals (9.5 mol% Y_2O_3, Crystec, Germany). The substrate was heated to temperatures of 700 – 800 °C during deposition and typical thicknesses of the deposited electrode films were between 400 and 500 nm (determined by ex-situ calibration using a quartz micro balance). In order to obtain microelectrodes with a diameter of 100 μm, the Pt films were micro-structured by standard photolithography (ma-N 1420 negative photoresist, micro resist technology, Germany), including an etching step in hot

nitro hydrochloric acid. The samples were subsequently annealed for 60 hours at 850 °C in air (58). Electrodes prepared by a similar route were already shown to be sufficiently stable from an (electro)chemical and geometrical point of view. (12)

The Pt thin film electrodes were investigated by scanning electron microscopy (SEM) on a Quanta 200 FEG (FEI Europe, The Netherlands) and the resulting micrographs are shown in Fig. 1. The images in Figs. 1a and b display the surface of a Pt thin film right after sputter deposition and after a 60 h annealing step at 850 °C, respectively. In both cases, Pt grain boundaries are clearly visible, indicating a polycrystalline growth of the Pt film. During the annealing process, some grain growth but no formation of pinholes took place. Also the formation of microscopic pores during the annealing step was excluded by higher magnified SEM images of the annealed films (cf. Fig. 1c). In Fig. 1d, circular shaped microelectrodes of different diameters are shown. In the present study, only the 100 μm electrodes (second largest electrodes in the image) were used for electrochemical measurements. The SEM image of the 100 μm electrode in Fig. 1e was recorded after extensive electrochemical measurements of the respective sample. However, the electrode itself was not used in these electrochemical experiments but was only exposed to the thermal treatment. A magnification of the electrode surface is depicted in Fig. 1f. The dark dots are precipitates or gas blisters of the Pt film rather than pores. From these results we conclude that the Pt films were sufficiently gas tight during the electrochemical measurements.

Further thin film characterization was done by x-ray diffraction (XRD) measurements on an X'Pert PRO Diffractometer (PANalytical, The Netherlands) with copper anode and X'Celerator detector with a Ni-K_β-filter. The diffraction pattern in Figs. 2a and b were obtained on a freshly deposited and an annealed Pt thin film on YSZ (100), respectively. Neglecting signals from some residual K_β-radiation, almost exclusively reflexes corresponding to YSZ (100) and Pt (111) could be detected on both films. Consequently, the Pt films were strongly (111) textured though not single crystalline, since grain boundaries are clearly visible in the SEM images (cf. Fig. 1). At 43.3 ° a weak reflex was found, which could neither be attributed to our YSZ substrate nor to Pt. However, the

corresponding impurity phase cannot be identified unambiguously from one single peak in the diffraction pattern.

2.2 Current-voltage measurements (dc)

For dc measurements at elevated temperatures, the samples were placed onto a heating stage (Linkam, UK). Electrical contact was established by Pt/Ir-tips (Suss, Germany) which could be precisely positioned under a microscope (Mitutoyo, Japan) by piezoelectric micromanipulators (Newport, USA). A sketch of the setup and a view through the microscope is shown in Fig. 3. To minimize deteriorating electrical effects of the heating stage during electrochemical measurements, a Pt sheet was introduced as shielding between sample and ceramic heating stage. The shielding was connected to ground potential of the analyzer. A thin sapphire disc was used to prevent conductive connection between sample and shielding.

The current-voltage measurements were performed using an Alpha-A High Performance Frequency Analyzer with POT/GAL 30V 2A test interface (Novocontrol, Germany) in dc mode (control software: Winchem, Novocontrol, Germany). Current voltage curves of 100 µm Pt electrodes were recorded between set temperatures of 700 and 850 °C in 25 °C steps. Owing to the asymmetric heating and the contact by the tip, the true electrode temperature differed from the set temperature by 100 – 120 °C. The true electrode temperature was calculated from the spreading resistance of ion conduction in YSZ (cf. Sec. 2.3) by the procedure described in Ref. (12). The temperature gradient within YSZ is known to be responsible for a thermovoltage (59), which was between 10 and 30 mV in the present study. This caused a shift of the current-voltage curves and had to be considered in the analysis of the dc experiments (cf. also Sec. 3.1).

For measuring I-η curves, the applied voltage was held constant for 200 s and the corresponding current was recorded every second. Between +0.1 and -1.5 V twenty-two voltage values were used. The anodic voltages were limited to +0.1 V in order to avoid irreversible morphology changes of the Pt electrodes such as bubble formation (31). Step size varied from 25 to

100 mV, with smaller step widths close to equilibrium. An exemplary curve showing the measured current as a function of measurement time is given in Fig. 4a. The I-t curves at each voltage set point show the typical relaxation characteristics of R-C elements. In order to exclude an effect of the charging current of the interfacial electrode capacitor, only the last 25 points, which almost exclusively reflect the faradayic current of the respective voltage, were averaged and taken into account for further analysis – cf. Fig. 4b. The voltage sequence was applied three times to check for any irreversible changes of the system upon polarization. In order to obtain the overpotential η of the Pt electrode, the contribution of the ohmic overpotential caused by YSZ had to be subtracted. However, since the voltage drop in the electrolyte was 0.1 mV or lower in all dc measurements of this study, $U_{set} \approx \eta$ can safely be assumed. The overpotential at the counter electrode was negligible due to its orders of magnitude larger size compared to the microelectrode (0.0079 mm² dense microelectrode vs. 10 mm² porous paste electrode) (60, 61).

2.3 Impedance measurements

Impedance measurements were performed on the same setup as described in Sec. 2.2. The POT/GAL 30V 2A test interface was set to ac mode (control software: Windeta, Novocontrol, Germany) and a pseudo-4-point technique with blocking capacitor was employed, since the thermovoltage mentioned above can lead to a polarization of the electrodes in a conventional 2-wire technique even for nominally zero bias; details are given in Ref. (34). The spectra were recorded in a frequency range between 500 kHz and 50 mHz at an ac voltage of 10 mV (rms).

In Fig. 5, the complex impedance plot of a spectrum obtained at 639 °C sample temperature is shown. In the temperature regime examined in the present study, the spectra consisted of three typical features: (i) A large semicircle dominates in the low frequency range, which in earlier studies was attributed to the rate limiting step of the electrode reaction proceeding in the close vicinity of the TPB (12, 34). (ii) In the medium frequency range a shoulder can be observed, which in a previous paper was interpreted in terms of an electrochemical process at the Pt|YSZ interface (12). Owing to

the huge difference in size between micro- and counter electrode, also this shoulder can be attributed to the Pt microelectrode (60, 61). (iii) In the high frequency region, the spectra exhibit an axis intercept which can be related to the spreading resistance of oxide ion conduction in the electrolyte (12, 61, 62).

3   Results and discussion

3.1   Parameterization of dc data

In Figs. 6a and 7a, current-overpotential curves obtained at different temperatures are depicted. Each curve shows results from one voltage cycle with the sequence 0.0 V $\rightarrow$ -1.5 V $\rightarrow$ +0.1 V $\rightarrow$ 0.0 V. In the anodic regime, an exponential increase of the current can be observed. In the cathodic branch, after a first increase, the current remains almost constant despite increasing overpotential. However, for very high polarization (voltages < -1 V), an exponential relationship between overpotential and current could be observed. Figs. 6b and 7b show the I-η data in a smaller voltage range (between +0.1 and -1.0 V) exhibiting the characteristic shape of mass transport limited kinetics with a limiting current (63). Similar I-η curves have already been reported in literature for different Pt electrodes on YSZ (porous Pt paste or point electrodes made by a Pt wire) at lower cathodic polarization values (18, 22, 30, 48, 64). An additional exponential current-overpotential relationship at high polarization, however, was not mentioned in those experiments. Such I-η curves could be obtained repeatedly at temperatures up to ca. 700 °C (electrode temperature). At higher temperatures, some irreversible changes of the electrodes during the measurements became obvious – see Fig. 7b (721 °C curve). Reasons for this irreversible behavior cannot be concluded from the data available so far and are not further investigated in the present study. The following analysis of the dc data is thus limited to measurements without such irreversible effects (usually below 700 °C electrode temperature).

The observed electrode characteristics with a limiting current at lower polarization and an exponential current-voltage relationship for high polarization, constitutes a quite unusual behavior. Commonly the reverse case is observed: exponential Butler-Volmer-like kinetics at low overpotential, followed by mass transport limitation when the polarization is increased. This situation can be described by a serial connection of two Faradaic processes and is often discussed in literature (63). In the present case, however, a parallel connection of two reaction paths is more appropriate to explain the measured shape of the I-η curves: A slow diffusion step leading to a limiting current in one path and an exponential process determining the current of the second path. The current-overpotential relation for diffusion limited kinetics and an exponential current-voltage relation are given by Eqs. 1 and 2, respectively (63):

$$I_{diff} = -I_{lim} \cdot \left(1 - e^{\frac{z_{diff} e_0}{k_B T} \eta} \right) \tag{1}$$

$$I_{exp} = -I_0 \cdot \left(e^{-\frac{b \cdot e_0}{k_B T} \eta} \right) \quad \text{for} \quad |b \cdot e_0 \cdot \eta| \gg k_B T \tag{2}$$

In Eq. 1, I_{diff} denotes the resulting diffusion current for a given overpotential η, I_{lim} is the limiting current, z_{diff} the number of electrons transferred by the diffusing particle, e_0 the elementary charge, k_B Boltzmann's constant and T the absolute temperature. In Eq. 2, I_{exp} denotes the current exponentially depending on the overpotential and I_0 and b are fitting parameters. For quantifying the exponential part of the I-η curve, the anodic reaction rate was neglected in Eq. 2; since the corresponding relation is only relevant for high cathodic overpotentials, its anodic contribution is irrelevant anyway. The total current I_{dc} resulting from a parallel connection of both processes is given by

$$I_{dc} = I_{diff} + I_{exp} \,. \tag{3}$$

To account for voltage shifts caused by the thermovoltage u_{therm} mentioned in Sec. 2.3, Eqs. 1 and 2 were further modified and by combining them with Eq. 3, the total dc current reads as follows:

$$I_{dc} = -I_{lim} \cdot \left(1 - e^{\frac{z_{diff} e_0}{k_B T} (\eta - u_{therm})} \right) - I_0 \cdot \left(e^{-\frac{b \cdot e_0}{k_B T} (\eta - u_{therm})} \right). \tag{4}$$

This equation was used to quantify the measured dc I-η curves. In the fitting procedure, I_{dc} and η were used as dependent and independent variable, respectively and the fitting parameters were I_{lim}, I_0, z_{diff}, and b. The value of the thermovoltage was measured before each dc measurement and used as a constant in the fit. Parameter T was the corrected electrode temperature (see Sec. 2.3). The resulting fit curves are compared with measurement data in Figs. 8 (661 °C) and 9 (701 °C) and demonstrate the satisfying description of experimental data by Eq. (4).

3.2 Diffusion limited reaction path

The fitting results of parameter I_{lim} are shown in the Arrhenius plot of Fig. 10a with different symbols indicating measurements on different electrodes. The values obtained on each electrode show acceptable Arrhenius-type behavior and all electrodes lead to similar activation energies with an average of 1.57 ± 0.17 eV. A rate-limiting diffusion process on the system Pt|YSZ was also frequently discussed in literature (15, 43), particularly in terms of a rate limiting surface diffusion of an adsorbed oxygen species on Pt or a co-limitation of surface diffusion and adsorption (35, 43, 65). Such co-limited kinetics associated with the Pt surface could be excluded for our Pt microelectrodes: In Ref. (34), the polarization resistance caused by adsorption was estimated from adsorption kinetics data and the resulting value is many orders of magnitude below the resistance measured on Pt model electrodes. However, a rate limiting diffusion step may also take place through an impurity "rim" at the TPB. This would also explain the large scattering of our data (cf. Fig. 10a), since different thicknesses, morphologies, porosities, or compositions of an impurity phase at the TPB of different electrodes are expected to lead to rather different polarization resistances.

In several studies, the TPB-related polarization resistance of Pt electrodes was indeed discussed to be influenced by impurities at the TPB (7, 10, 34, 66), even though impurity related resistances were mostly not specified in terms of a diffusion limitation. In Refs. (7, 10) Si containing impurities were explicitly shown to drastically affect oxygen exchange kinetics of Pt electrodes on YSZ. For example, it was demonstrated that Si-free electrodes had tremendously lower polarization

resistances than Si containing ones. Moreover, the polarization resistances of the Si-contaminated electrodes showed much more scattering than those of Si free electrodes (7). Accordingly, we regard the similar behavior found in our experiments as a strong indication of an impurity phase at the TPB causing the diffusion limited reaction path.

Since the pre-exponential factor I_0 of the exponential-type reaction path (Eq. 2) is orders of magnitude lower than the diffusion limiting current, the polarization resistance close to equilibrium $R_{ac,eq}$ can simply be calculated by differentiating the diffusion related part of Eq. 4

$$\frac{1}{R_{ac,eq}} = \frac{dI_{diff}}{d\eta}\bigg|_{\eta=u_{therm}} = I_{lim} \cdot \frac{z_{diff}e_0}{k_BT} \cdot e^{\frac{z_{diff}e_0}{k_BT}(\eta-u_{therm})}\bigg|_{\eta=u_{therm}} = I_{lim} \cdot \frac{z_{diff}e_0}{k_BT} . \tag{5}$$

The resulting inverse polarization resistance can be normalized to the TPB-length of the electrodes and compared to the results of an impedance study, measured without bias voltage on similarly prepared Pt microelectrodes of 100 μm diameter (12); cf. Fig. 11. Also in this previous study, a remarkable scattering of the polarization resistances was observed (12) and only averaged values are shown in Fig. 11. From this comparison it becomes obvious that the values determined from the dc results by Eq. 5 scatter around the averaged values obtained from ac measurements. Both data sets exhibit very similar activation energies. This good (and expected) agreement shows that the TPB-related polarization resistance measured above 600 °C in our previous studies (12, 34) can be attributed to the same diffusion-limited process as the dc data shown here, i.e. most probably to impurity related diffusion limitation.

The second fit parameter z_{diff} also showed a broad distribution of values for different electrodes, but in contrast to I_{lim} clear trends in dependence of temperature could not be identified (Fig. 10b). Reasons for this scattering as well as for the average value of roughly one are not clear. Thus, more detailed information on the exact path (through the phase, along an interface between impurity phase and electrode, etc.) and on the diffusing species cannot yet be deduced from z_{diff}.

3.3 Path exhibiting an exponential current-voltage relationship

3.3.1 General considerations

Both fitting parameters (I_0 and b) related to the exponential part of the fit function are depicted in Fig. 12 for different electrodes of 100 μm diameter; the results of I_0 are shown in an Arrhenius plot. (Two measurements were not considered due to problems with the fitting procedure). I_0 exhibits an activation energy of 3.65 ± 0.35 eV, which is uncommonly high for electrode processes on YSZ. The average value of fitting parameter b was 1.05 ± 0.07. Interestingly, the absolute values of I_0 scatter much less than those of I_{lim}.

It was already discussed in Sec.3.1 that such an exponential behavior is very likely attributed to a path in parallel to the diffusion limited reaction path of Sec. 3.2. A bulk path through Pt and a YSZ surface path with oxygen incorporation at the free YSZ surface are possible scenarios - see Fig. 13. According to Refs. (34) and (56), a bulk path through Pt – (c) in Fig. 13 – indeed exists, but is limited by diffusion of oxygen along Pt grain boundaries and only relevant at temperatures below 450 °C. Therefore, the observed exponential I-η relationship is attributed to the reaction path with oxygen being incorporated on the free YSZ surface ((b) in Fig. 13). In such a surface path, electron conduction in YSZ from Pt to the oxygen reduction sites on the free YSZ surface is required. The exponential relationship between current and voltage upon high polarization may be interpreted in at least two different ways: (i) Changes in the local electronic conductivity of YSZ caused by cathodic reduction of YSZ (stoichiometry polarization) could lead to an exponential current-voltage relationship (see Sec. 3.3.2). (ii) Charge transfer limited electrode kinetics would be another possibility leading to the observed exponential current-voltage behavior (63) and the high activation energy, see 3.3.3.

3.3.2 Stoichiometry polarization

The conductivity of electrons in YSZ is proportional to their concentration (assuming that their mobility is concentration independent) (67, 68). The stoichiometry of YSZ and thus the concentration of mobile electrons in the material can be changed by electrochemical polarization. The electronic current I_{eon} through YSZ, resulting for one electrode being ideally blocking to the ionic current and a reversible counter electrode (classical Wagner-Hebb polarization), is given by (69)

$$I_{eon} = -\frac{k_B T}{e_0 B} \cdot \sigma_{eon,eq} \cdot e^{-\frac{e_0}{k_B T}\eta} \text{ for } |e_0\eta| \gg k_B T \, . \tag{6}$$

In Eq. (6), B denotes the length of a quasi-one-dimensional sample and $\sigma_{eon,eq}$ is the electronic conductivity of YSZ upon equilibrium conditions (i.e. at the reversible electrode).

A very similar situation is found in our case: The Pt microelectrode is electrochemically highly resistive, though not entirely blocking for oxygen exchange along the TPB, while the counter electrode is virtually reversible. Accordingly, a significant stoichiometry polarization beneath the Pt electrode can be expected. From the resulting potential distribution (70) it can be concluded that the stoichiometry variation is most pronounced at the TPB and is decaying along the free electrolyte surface. The related increase of the local electron concentration in YSZ close to the Pt electrode can open the pathway for oxygen reduction on the free YSZ surface. For rate limiting electron conduction from Pt to the reaction sites on YSZ, an I-η relation similar to Wagner-Hebb polarization is expected. The relevant geometrical parameter B' (replacing B in Eq. 6) then reflects the lateral path of electrons from Pt to the reaction site rather than the distance to the counter electrode. Hence, despite our electrode setup is not quasi-one-dimensional and the Pt microelectrode is not ideally blocking, we regard Eq. 6 as a reasonable approximation, describing the I-η behavior in case of electron transport in YSZ as the rate limiting step of oxygen reduction on the free YSZ surface.

In this interpretation, the fitting parameter b in Eq. 2 has to be unity and the parameter I_0 reads (compare Eqs. 2 and 6)

$$I_0 = \frac{k_B T}{e_0 B'} \cdot \sigma_{eon,eq} \, . \tag{7}$$

Accordingly, the activation energy of I_0 should be given by the activation energy of electron conduction in YSZ. The activation energy of I_0 (3.65 ± 0.36 eV) obtained from the Arrhenius fit in Fig. 12a is indeed in good agreement with activation energy values reported for electronic conductivity in stabilized zirconia, e.g. 3.88 eV for 8 mol% Y_2O_3-ZrO_2 (68) and 3.7 eV for 15 mol% CaO-ZrO_2 (71). Since also the fit parameter $b = 1.05 \pm 0.07$ (cf. Fig. 12b) is in excellent agreement with this model, we consider electron conduction in YSZ to be a very likely rate limiting process causing the exponential part of the current-voltage characteristics of our Pt electrodes. A YSZ surface path was already reported for the system noble metal (Au; Pt)|Sm-doped ceria in hydrogen atmosphere (72).

In case of an ideally ion-blocking electrode, the relationship between current and set voltage would also be exponential, because of electronic current still flowing through YSZ from the ion-blocking to the reversible electrode; cf. Eq. 6. To exclude this classical Wagner-Hebb-like electronic current as the source of our exponential current-voltage behavior, an impedance spectrum measured under -1.5 V bias is compared to a spectrum obtained without an additional dc voltage (Fig. 14). The high frequency axis intercepts of both spectra are virtually the same and correspond to the spreading resistance of ion conduction in YSZ (12, 61, 62). A substantial electronic current flow between the microelectrode and the counter electrode would significantly affect the total YSZ resistance, i.e. the high frequency intercept in the impedance spectrum. Hence, the current in YSZ is still almost exclusively ionic, even for -1.5 V bias. However, according to this model a significant electronic current flows within YSZ from Pt to the reaction sites on the YSZ surface; those sites are expected to be still close to the Pt microelectrode, and the resistance thus TPB related. This electronic current is strongly enhanced by the stoichiometry polarization close to the microelectrode. At the free YSZ surface, the electrochemical oxygen reduction reaction transfers this lateral electronic current into an ionic current I_{exp} which then flows from the reaction site to the counter electrode.

3.3.3 Polarization due to charge transfer and low electron concentration in YSZ

Another process possibly leading to an exponential I-η curve is the charge transfer reaction

$$O^{y} + e^{-} \underset{anodic}{\overset{cathodic}{\rightleftharpoons}} O^{y-1} \tag{8}$$

on the free YSZ surface (O^{y} denotes an arbitrary oxygen species with charge y). The exchange current I_{eq} of such a reaction is given by

$$I_{eq} = e_{0} \cdot k_{cath} \cdot \left[O^{y} \right]_{eq} \cdot \left[e^{-} \right]_{eq} \tag{9}$$

with k_{cath} denoting the rate constant of the cathodic reaction, $[O^{y}]_{eq}$ the equilibrium concentration of the oxygen species and $[e^{-}]_{eq}$ the equilibrium concentration of electrons in YSZ. YSZ acts as a mixed ionic and electronic conductor in this path and the charge transfer kinetics on such mixed conductor surfaces is highly complex (73): The variation of the relevant surface potential difference is not identical to the overpotential and further, in contrast to classical Butler-Volmer kinetics, the concentrations cannot be assumed to be independent of η. The electron concentration changes due to stoichiometry polarization (cf. 3.3.2) and the concentration of any charged oxygen species on the YSZ surface should depend on the surface potential difference of YSZ, which is coupled to η by non-trivial relationships (73). Thus, a straightforward discussion of I-η relationships cannot be given at this point. Also an estimation of the corresponding activation energy is difficult even though very high values can again be expected, simply due to the highly temperature dependent electron concentration (68, 71). Hence, also a charge transfer reaction at the YSZ surface cannot be excluded as rate limiting step of the exponential part in the I-η curves. Nevertheless, we regard rate limiting electron conduction as the more probably scenario, due to both its excellent agreement in activation energy and the assumable comparability with the system noble metal|Sm-doped ceria.

3.4 Consequences for the quantification of impedance spectra

It was already mentioned above that the I-η curve close to equilibrium corresponds to the situation observed in impedance measurements without bias voltage. In agreement with previous

impedance measurements (12, 34), again a large arc in the complex impedance plane was observed (Fig. 5) and this arc is mainly caused by the diffusion limited process discussed in Sec. 3.2. However, as in Ref. (12), a kind of shoulder was found at high frequencies. This cannot be explained by the reaction paths discussed so far for dc measurements. The corresponding resistance is proportional to the inverse electrode area (12) and thus neither caused by an additional step in the diffusion limited TPB path nor related to the path originating at the free YSZ surface. The latter is not only dependent on the TPB length, but also negligible close to equilibrium. Hence, in the investigated temperature region between 600 and 700 °C, the complete picture of electrochemical reaction paths on Pt thin film electrodes has to consider the following reaction pathways (sketched in Fig. 13): The diffusion limited TPB path, presumably across an impurity phase (a), the YSZ surface path measurable only at high overpotentials (b), a bulk path along grain boundaries only relevant at low temperatures (34) (c) and a fourth path visible as high frequency shoulder in the impedance spectra (d). Since the resistance of this fourth path is much smaller, compared to that of the parallel Pt surface path, but not relevant in small signal dc measurements, it can be assumed to be capacitively blocked. Moreover, a purely capacitive path via the interfacial capacitor (74, 75) has to be considered in analysis of ac data (e).

In our impedance study on similar Pt microelectrodes (12), the equivalent circuit in Fig. 15a was used for analysis. It consists of an R_1-CPE_1 element, with CPE denoting a constant phase element and R_1 being caused by path (a), in parallel to an additional capacitively blocked reaction path (d) and to the interfacial capacitor (e). As a possible interpretation of this capacitively blocked path (high frequency shoulder in the spectra), an electrochemical reaction of "chemisorbed" oxygen at the Pt|YSZ interface was suggested, which might be attributed to an interfacial nonstoichiometric impurity phase or to an interfacial oxide phase of Pt. In Fig. 15a, the Bode plot of the impedance spectrum in Fig. 5 (open circles) is compared to the complex non-linear least squares (CNLS) fit employing the sketched circuit. The low frequency part of the spectrum (reflecting the polarization resistance of the rate determining step) is described with sufficient accuracy, whereas some deviation between fit and measured data can still be observed in the medium and high frequency

range. This deviation is not surprising, since the corresponding equivalent circuit does not yet consider circuit elements in accordance with the more detailed mechanistic interpretation of the dc data given in this study. Since the main arc in the spectrum was attributed to a rate limiting diffusion, a generalized finite Warburg (GFW) element (76) should be used instead of resistor R_1 in Fig. 15a. For a short circuited terminus, the impedance Z_{GFW} of the GFW element is defined by

$$Z_{GFW} = \frac{R_{GFW} \cdot \tanh\left(i \cdot \omega \cdot \tau\right)}{\left(i \cdot \omega \cdot \tau\right)^p} \tag{10}$$

where i and ω are the imaginary unit and the angular frequency, respectively. R_{GFW}, τ and p are fitting parameters. In the diffusion interpretation with p = 0.5, R_{GFW} is the dc diffusion resistance and τ is a characteristic time given by

$$\tau = \frac{L^2}{D} \tag{11}$$

with L denoting the diffusion length and D the diffusion coefficient.

However, the accuracy of a fit using a GFW element instead of R_1 increases only slightly. When also replacing the second resistor R_2 by a GFW element (see Fig. 15b), the fit quality becomes considerably higher, particularly at higher frequencies. The results of the CNLS-fit for this equivalent circuit are compared with the measured data in Fig. 15b and fit parameters are summarized in Tab. 1. Since the p values of both Warburg elements are not far from 0.5 (0.65 for GFW_1 and 0.44 for GFW_2), both may still be interpreted as non-ideal diffusion processes. Despite the only moderate errors for all fit parameters in Tab. 1, it remains an open question, whether this modification of the equivalent circuit is an over-parameterization or has a physical meaning. Nevertheless, a few aspects regarding the mechanistic relevance of the elements of this circuit are worth mentioning: The significance of element GFW_1 (as already discussed above) is in accordance with the dc results. The semicircle-like appearance of the electrode impedance rather than a 45° line in the high frequency part of the Nyquist plot (which would be expected for diffusion processes), despite a Warburg element, can be attributed to the relatively high value of the interfacial capacitor represented by CPE_1: approximately

50 µF/cm² was found in this study, which is a high but still reasonable value for double layer capacitances in the observed temperature range (74).

The capacitively blocked diffusive path (d) in parallel to the TPB-processes (see Figs. 13 and 15b) might be related to a PtO_x "phase". PtO_x as a potential source for an electrochemical process at the Pt|YSZ interface was already discussed in several studies (6, 11, 18, 40). In Ref. (6), a diffusion controlled process was suggested for anodic growth of PtO_x at the interface. Assuming the existence of such a PtO_x "phase" also close to equilibrium conditions, a capacitively blocked GFW element instead of a resistor could indeed be a reasonable approximation of a more complex circuit describing stoichiometry polarization of a mixed conducting phase (77). However, from the data available so far, the existence of PtO_x at the interface could not be proven unambiguously.

3.5 Extrapolation to lower temperatures and relevance for ¹⁸O tracer experiments

From the measured data (I-η relations and activation energies) we can extrapolate the currents of the two TPB-related paths (a) and (b) to lower temperatures. This is also interesting in the context of recent voltage-driven ¹⁸O tracer incorporation experiments (13, 78), which allowed quantification of the electrochemically active TPB width at temperatures of about 300 °C and high cathodic overpotentials. In Fig. 16a, extrapolated Arrhenius plots of the two equilibrium polarization resistances, identified in the dc measurements of this study (i.e. the inverse derivatives of Eqs. 1 and 2 at η = 0 V), are shown for the temperature range of 275 – 750 °C. This graph clearly indicates that around equilibrium the path with a rate limiting oxygen diffusion process through an impurity phase is the dominating TPB-related path in the entire temperature range. In Figs. 16b-f, Arrhenius plots of the dc currents calculated by Eqs. 1 and 2, are shown for different overpotentials. Up to cathodic polarization of -1.0 V, the diffusion limited Pt surface path is still carrying the major part of the current (cf. Figs. 16b-d). At higher cathodic polarization (-1.5 V, Fig. 16e), however, the YSZ surface path starts to outperform the Pt surface path. A further increase in polarization to -2.0 V leads to a

situation, where the YSZ surface path is carrying an orders of magnitude higher current in the entire temperature range (Fig. 16f).

In Ref. (13), it was shown by means of voltage-driven ^{18}O tracer experiments that the electrochemically active region of oxygen incorporation into YSZ at relatively high cathodic overpotentials (ca. -2 V) and low temperatures (ca. 300 °C) includes a frame-shaped zone close to the TPB with high incorporation rate. High cathodic polarization values were necessary in that study in order to get sufficient ^{18}O incorporated into YSZ. The width of the incorporation zone could be quantified and amounts to 1.0 – 1.3 μm between overpotentials of -1.99 and -2.22 μm (13). However, it remained an open question, whether the process leading to this TPB width was the same as the elementary step determining the TPB-related resistance close to equilibrium at higher temperatures. From the extrapolations shown in Fig. 16, it can now be concluded that the TPB process visualized in the ^{18}O tracer experiments in Ref. (13) was almost exclusively related to the YSZ surface path. This conclusion is also supported by the following quantification: From the ^{18}O intensities close to the TPB measured in Ref. (13), the current via the YSZ surface path can be calculated. In Fig. 16f the corresponding current (extrapolated to a circular 100 μm electrode) is shown by the blue cross at 308 °C. It is indeed in very good agreement with the dc current via the YSZ surface path measured in the present study. (It should be noted that only a slight change in the activation energy of the process on the YSZ surface – 3.72 eV instead of 3.65 eV – yields exactly the current value of Ref. (13). This is still within the statistical scatter of the value obtained for I_0 in Fig. 12: 3.65 ± 0.36 eV). This result seems to contradict the conclusion in Ref. (13) that the oxygen incorporation zone close to the TPB is located underneath the Pt electrode. Reasons for oxygen being apparently incorporated in a TPB-near zone underneath the Pt electrodes in Ref. (13), however, are not clear. The exact locations of the oxygen incorporation zones of both TPB-related pathways are thus still open questions.

4 Conclusions

In this dc study on Pt model electrodes, it was demonstrated that in electrochemical equilibrium and for low cathodic polarization a slow mass transport process at the TPB is the rate limiting elementary step of oxygen exchange. This transport limitation is most probably caused by oxygen diffusion through or along an additional phase (probably impurities) at the TPB of the Pt electrodes. Both, the resulting differential resistance around equilibrium and the activation energy (1.57 ± 0.17 eV) of the diffusion limiting current are in reasonable agreement with results of previous studies on Pt|YSZ (12, 14, 22, 34, 79). At sufficiently high cathodic polarization, a parallel reaction path becomes relevant, which shows an exponential dependence of the current on the overpotential. This exponential part of the I-η curve could be related to oxygen reduction via the free YSZ surface and was interpreted in terms of rate limiting electron conduction in YSZ. This conclusion is also in accordance with the similar activation energies of the electrochemical process (3.65 ± 0.36 eV) and the electronic conductivity in YSZ. Moreover, from the extrapolation of dc results to lower temperatures and higher cathodic polarization, it was possible to relate the TPB process observed in previous ^{18}O incorporation experiments to the YSZ surface path with oxygen reduction on the free electrolyte surface.

This completes the picture of different electrochemical reaction pathways on the $Pt(O_2)$|YSZ system: i) A Pt surface path with diffusion limitation probably due to an impurity phase at the TPB, ii) a YSZ surface path only relevant for very high polarization, iii) a Pt bulk path only relevant for low temperatures, and iv) a capacitively blocked reaction at the YSZ/Pt interface. Depending on temperature, electrode preparation, sample history, and overpotential these paths may contribute to a higher or lower degree to the data measured in impedance and dc studies. Accordingly, oxygen exchange kinetics on Pt|YSZ is definitely more complex than often assumed in literature.

Acknowledgement

Tables

Table 1: Comparison of CNLS-fit results obtained from fits of the spectrum in Fig. 5 with two different equivalent circuits. The measurement and the respective fit result are compared in the Bode plots in Fig. 15. (Denotation of fit-parameters: The χ^2 is the square of the standard deviation between the original data and the calculated spectrum. The Σ of sqr is the weighted sum of squares, which is proportional to the average percentage error between the original data points and the calculated values. R_{YSZ} is the spreading resistance of ion conduction in the electrolyte. CPE-Q and CPE-n are the fit-parameters of a constant phase element with the complex impedance $Z_{CPE} = (i\omega)^{-n} \cdot Q^{-1}$. GFW-R, GFW-$\tau$ and GFW-p are the fit parameters of a generalized finite Warburg element – compare Eq. 10. R and C denote resistors and capacitors, respectively.)

equivalent circuit from Ref. (12)			equivalent circuit considering diffusion limitations		
fit-parameter	value	fit-error / %	fit-parameter	value	fit-error / %
χ^2	1.53×10^{-3}	—	χ^2	6.21×10^{-5}	—
Σ of sqr	0.1377	—	Σ of sqr	0.0049	—
R_{YSZ} / Ω	6409	0.46	R_{YSZ} / Ω	6288	0.16
R_1 / Ω	3.13×10^7	0.99	GFW_1-R / Ω	3.11×10^7	0.26
			GFW_1-τ	3.72×10^{-2}	6.27
			GFW_1-p	0.6451	2.78
CPE_1-Q	1.58×10^{-8}	1.51	CPE_1-Q	1.38×10^{-8}	1.00
CPE_1-n	0.9098	0.18	CPE_1-n	0.8950	0.15
R_2 / Ω	86216	5.20	GFW_2-R / Ω	57481	4.41
			GFW_2-τ	6.02×10^{-4}	5.72
			GFW_2-p	0.4391	2.11
C_2 / F	3.88×10^{-9}	3.08	C_2 / F	5.47×10^{-9}	1.84

Figures
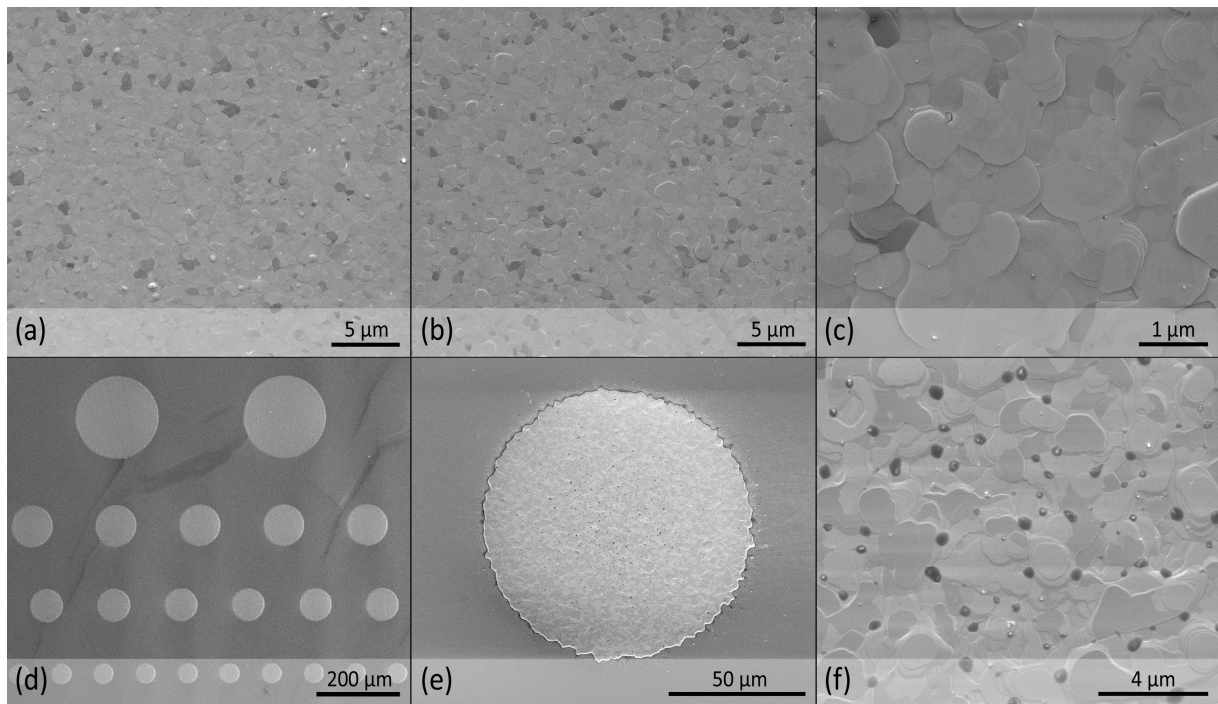
Figure 1: SEM images of Pt thin film electrodes. (a) Pt surface directly after sputter deposition. (b) Pt surface after 60 h annealing at 850 °C. (c) Higher magnification of (b) – Pt grain boundaries but no pores are visible. (d) Photolithographically micro-patterned Pt electrodes with different diameters. The 100 µm electrodes (second row from top) were used in the present study. (e) Magnification of a 100 µm electrode on a sample after electrical measurements; the electrode itself was not used in these measurements. (f) Surface of the electrode in (e).
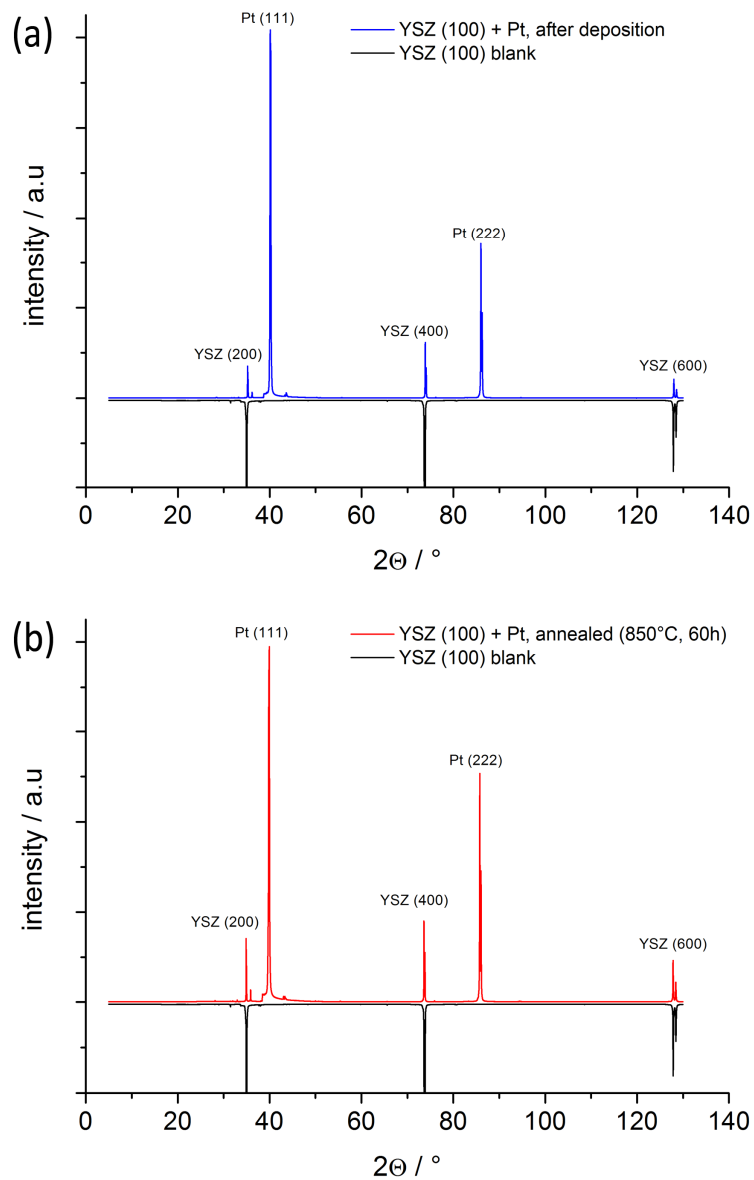
Figure 2: Diffraction pattern of sputter deposited Pt thin films on YSZ (100). (a) XRD measurement directly after thin film preparation compared with a YSZ blank measurement (mirrored). (b) Measurement after a 60 h annealing step at 850 °C.
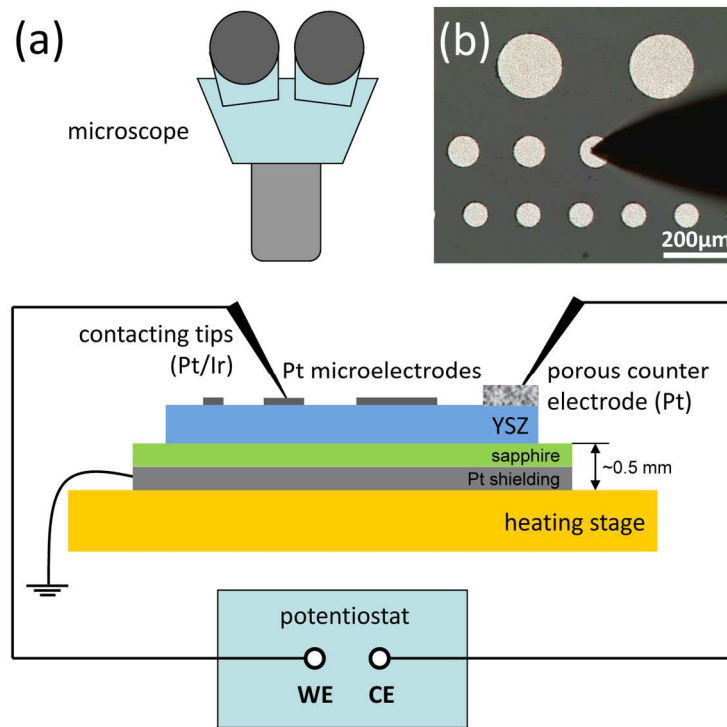
Figure 3: (a) Sketch of the dc-measurements setup. The labels of the connectors on the potentiostat denote working electrode and counter electrode, respectively. (b) View through the microscope with a 100 μm microelectrode contacted by a tip.
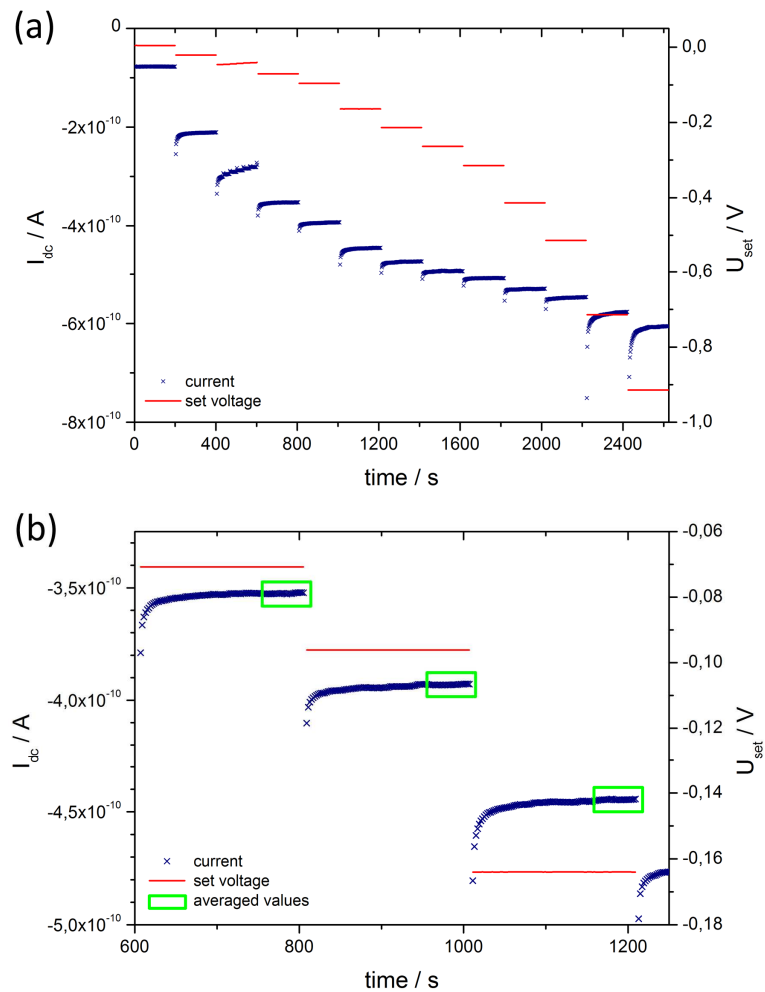
Figure 4: (a) Measured current (left y-axis) and voltage (right y-axis) plotted as a function of time. The diagram shows the interval between the start of the experiment and a cathodic polarization of -0.9 V. The holding time at each set voltage was 200 s. (b) Magnification of three I-t characteristics (at three voltage set points) showing the typical relaxation characteristics of R-C elements (i.e. charging of the interfacial capacitance). The green boxes denote the part of the curves used for averaging.
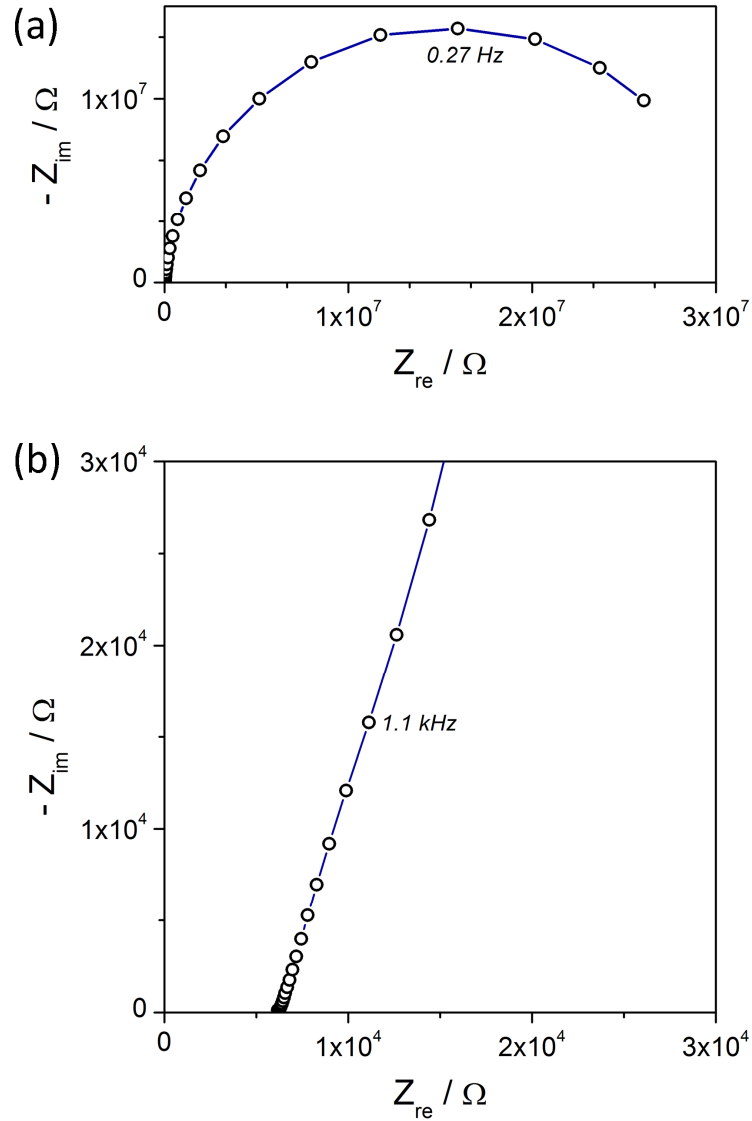
Figure 5: Impedance spectrum (Nyquist plot) of a 100 μm Pt electrode measured at 639 °C (real temperature). (a) High frequency part of the spectrum showing the dominating arc. (b) Low frequency part displaying a real axis intercept and a medium frequency shoulder.
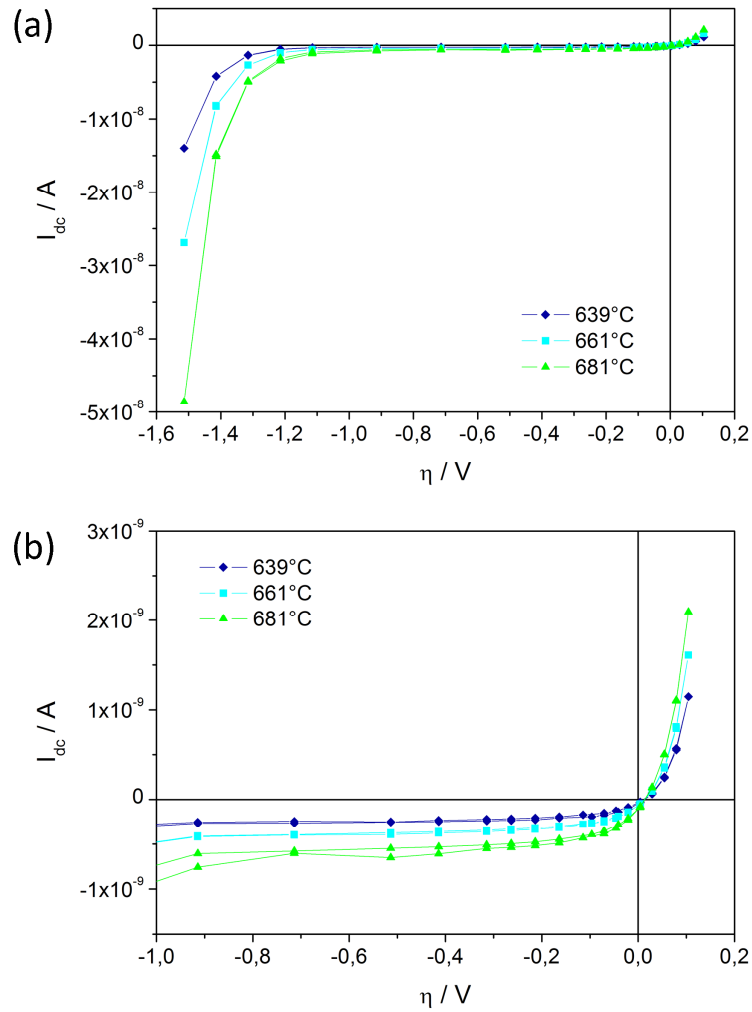
Figure 6: (a) Current-overpotential curves (one cycle) measured on 100 μm electrodes at 639 °C (dark blue diamonds), 661 °C (light blue squares), and 681 °C (green triangles). The given temperatures denote corrected values (cf. Sec. 2.3). (b) Magnification of the less polarized part of the curves in (a).
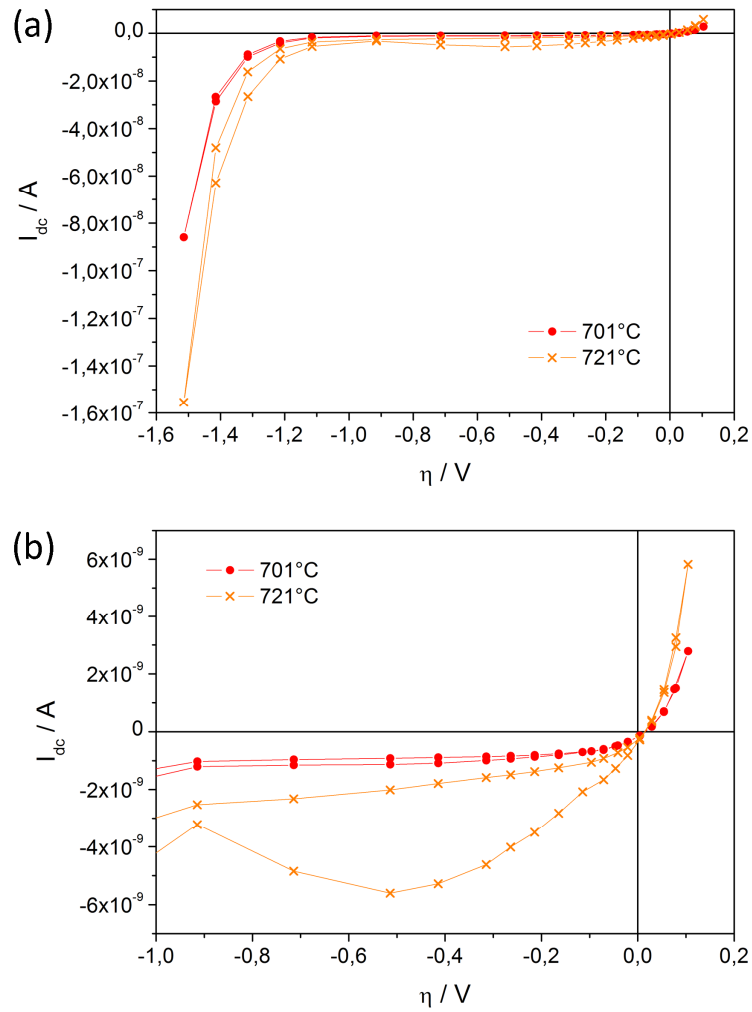
Figure 7: (a) Current-overpotential curves (one cycle) measured on 100 μm electrodes at 701 °C (red circles), and 721 °C (orange crosses). The given temperatures denote corrected values (cf. Sec. 2.3). (b) Magnification of the less polarized part of the curves in (a).
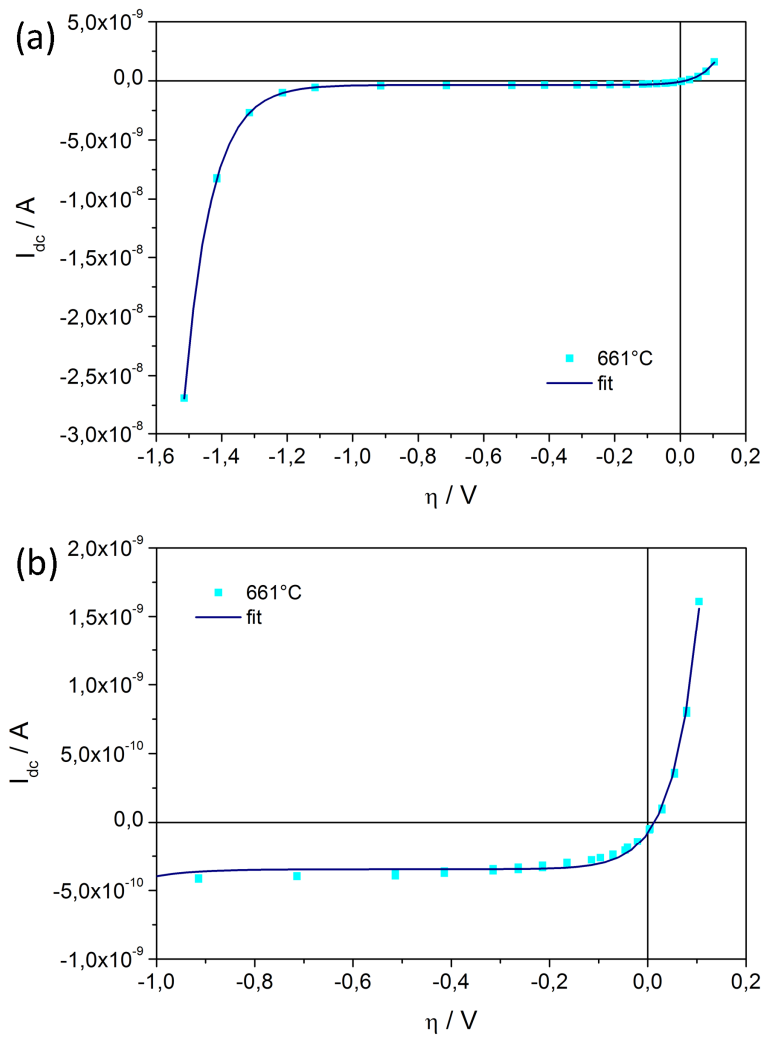
Figure 8: The 661 °C curve from Fig. 6 together with the fit curve according to Eq. 4. (a) Entire voltage range. (b) Diffusion dominated part at lower polarization.
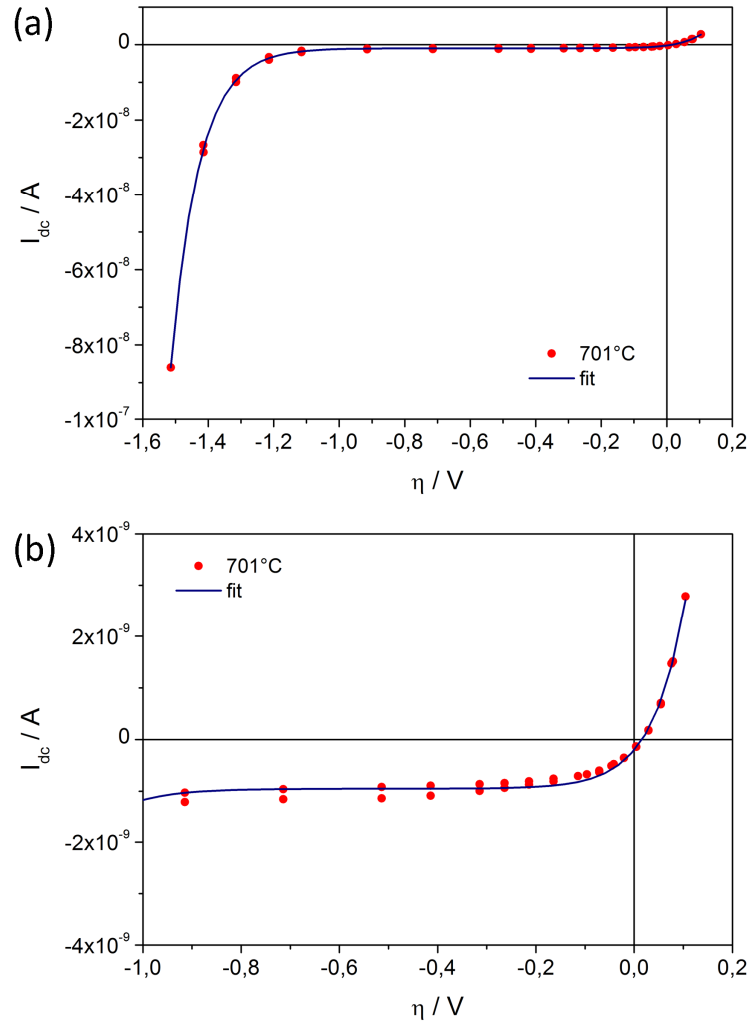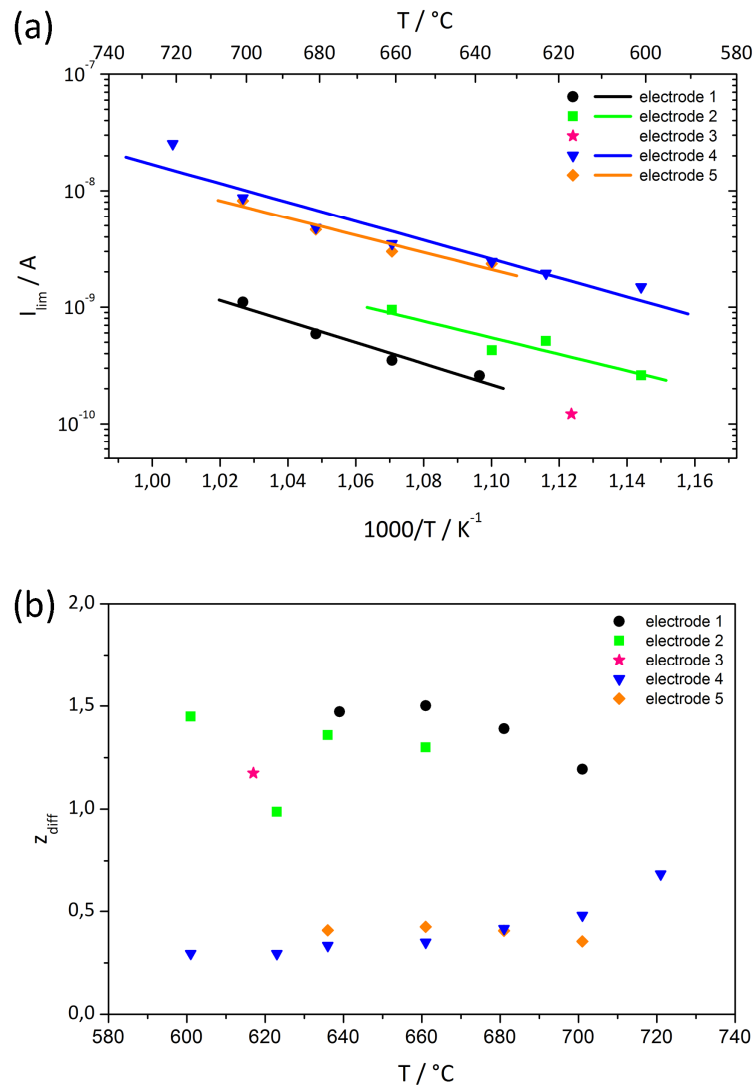
Figure 9: The 701 °C curve from Fig. 7 together with the fit curve according to Eq. 4. (a) Entire voltage range. (b) Diffusion dominated part at lower polarization.

Figure 10: Fit parameters corresponding to the diffusion related process (cf. Eq. 1). (a) Arrhenius plot of the limiting current I_{lim} (absolute values) including linear regression lines. Different symbols correspond to different electrodes. (b) Plot of z_{diff} values versus temperature.
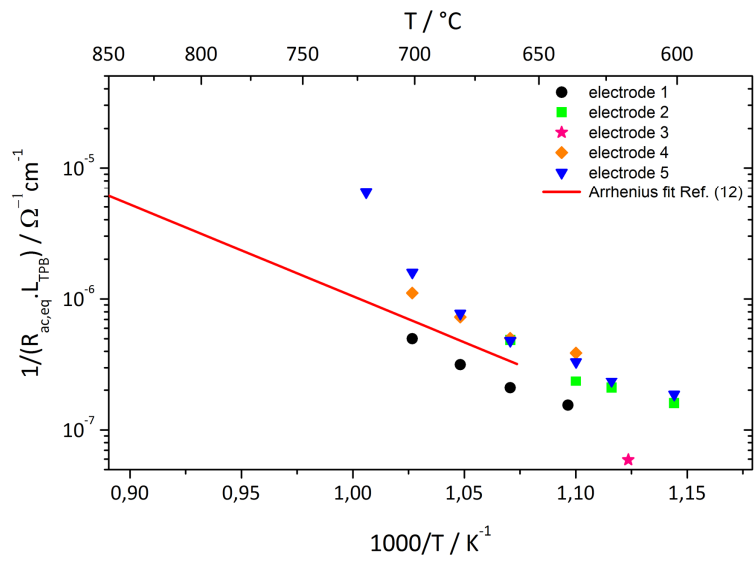
Figure 11: Comparison of TPB-length related inverse polarization resistances (obtained from the slopes of the fit curves at η = u_therm) with results of impedance data from Ref. (12). The values in Ref. (12) were obtained on similarly prepared 100 μm Pt electrodes.
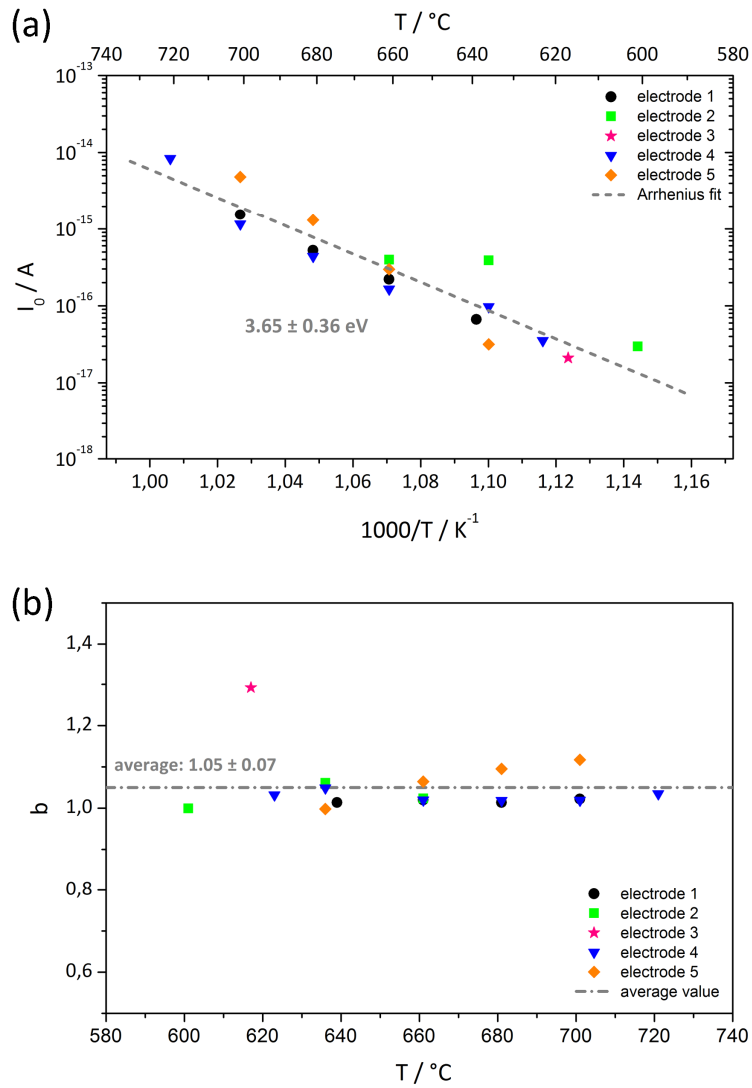
Figure 12: Fit parameters corresponding to Eq. 2 for different electrodes. (a) Arrhenius plot of the fit parameter I_0. Taking the data of all electrodes into account the grey dashed fit line is obtained; (b) Plot of b values versus temperature; the average value of all data points is indicated as gray dash-dotted line.
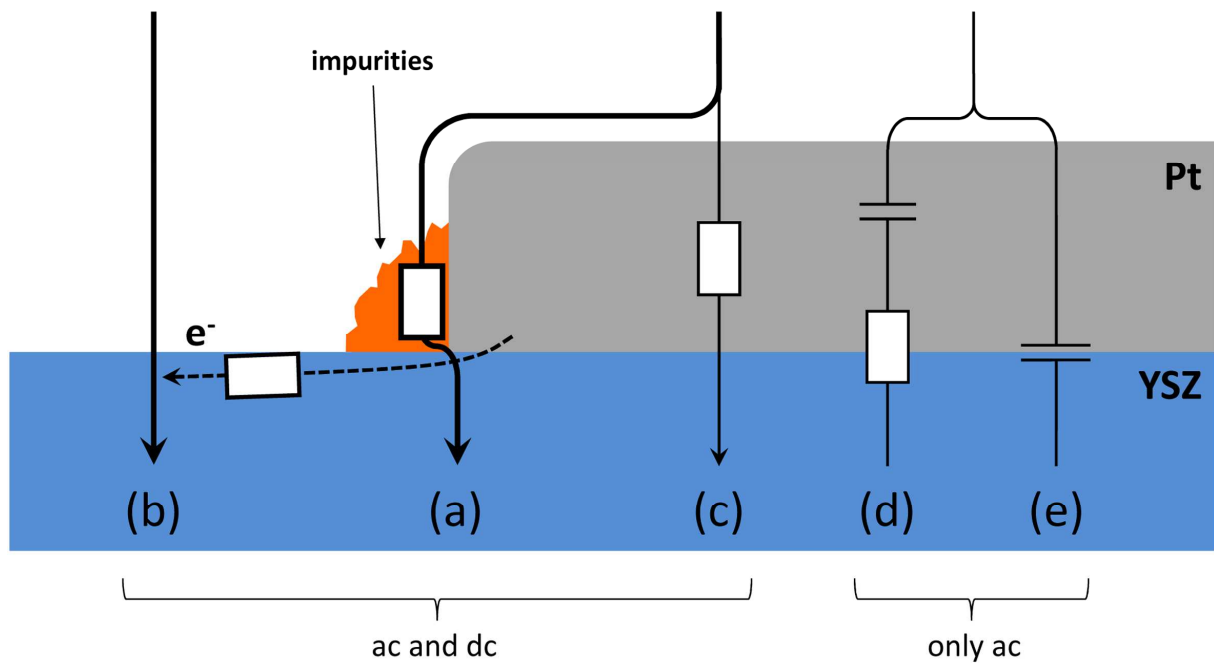
Figure 13: Sketch of the discussed parallel electrochemical pathways: (a) Pt surface path with diffusion of oxygen through an impurity phase at the TPB being rate limiting, determining the low polarization part of this dc study. (b) Electrochemical oxygen reduction process on the free YSZ surface with electron supply via the electrolyte, determining the high polarization part of this dc study. (c) Pt bulk path with rate limiting oxygen transport along grain boundaries of Pt (only relevant at low temperatures). (d) Capacitively blocked path via the electrochemical reduction/oxidation of a PtO_x "phase" at the Pt|YSZ interface. (e) Interfacial (double layer) capacitor.
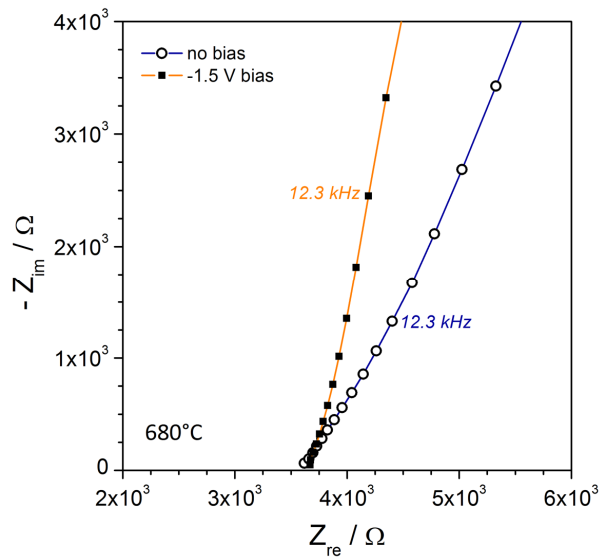
Figure 14: High frequency part of impedance spectra measured without an additional dc bias (open circles) and at -1.5 V bias (filled squares). The high frequency intercept is virtually the same indicating absence of any noteworthy electronic current in parallel to the ionic current in YSZ.
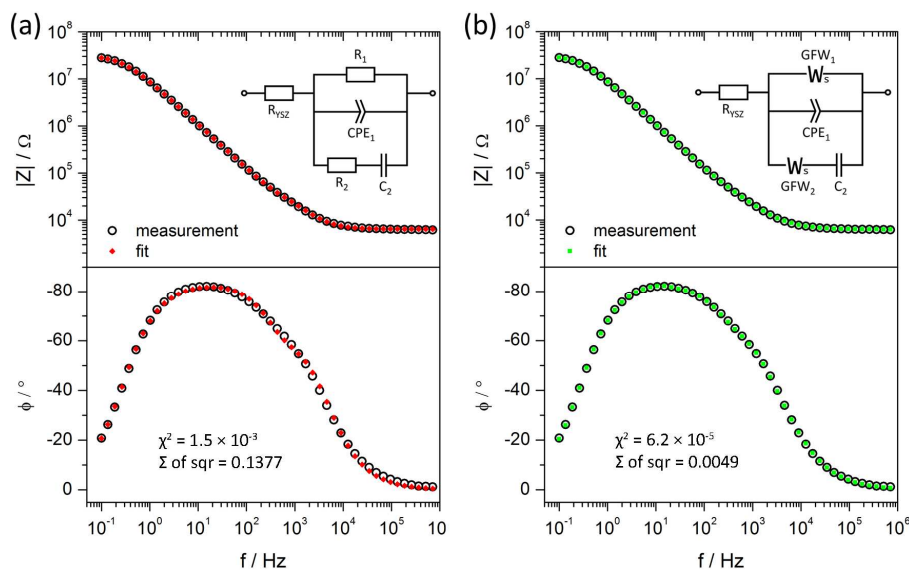

Figure 15 Bode plots of the measured impedance spectra in Fig. 5 (open circles) compared to the fits using two different equivalent circuits (depicted as inserts). (a) For the equivalent circuit from Ref. (12). (b) Using a modified equivalent circuit considering diffusion limitations as described in the text.
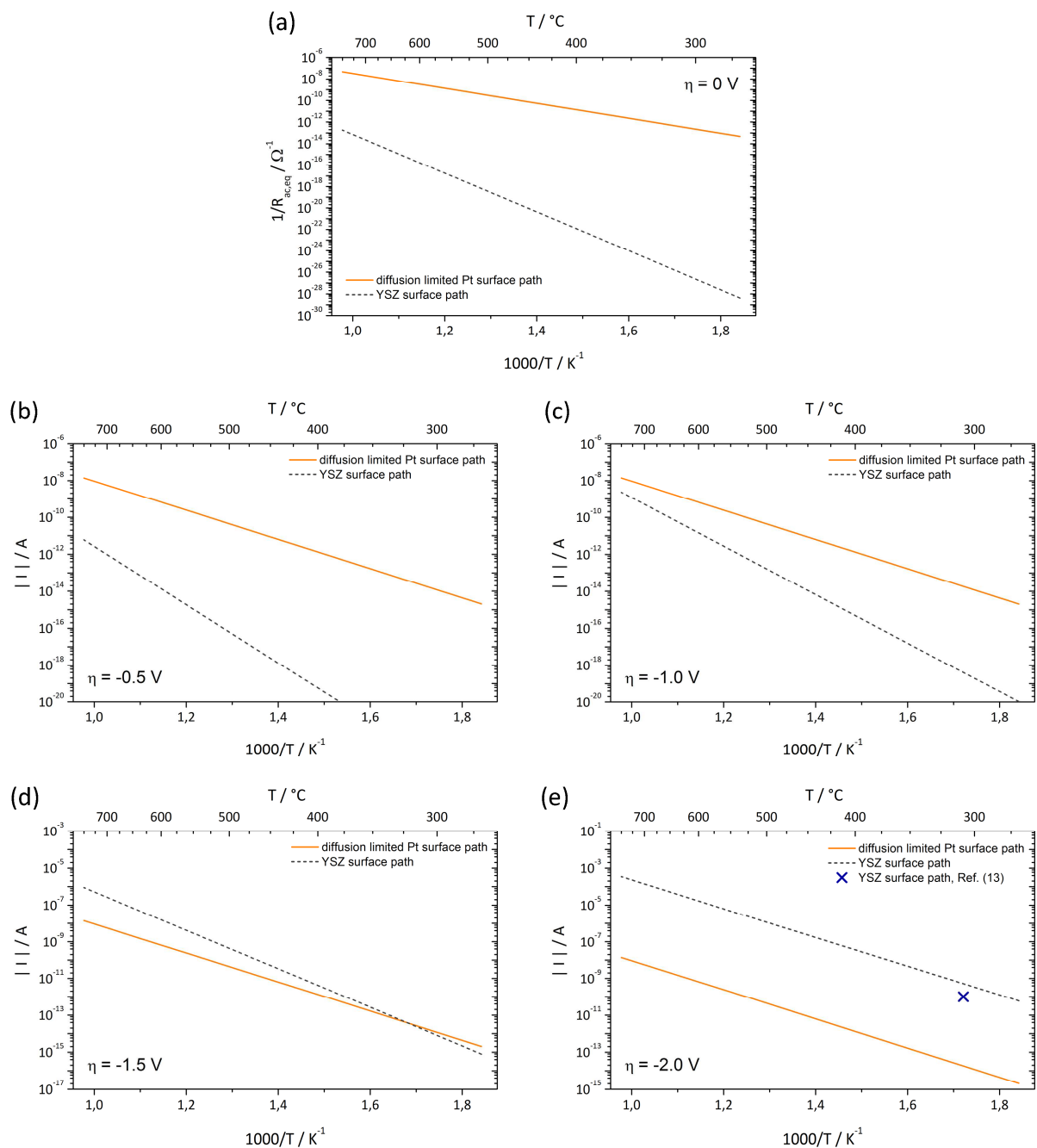
Figure 16: Arrhenius plots for the two processes identified in dc experiments and extrapolated to lower temperatures. The orange continuous line reflects the diffusion limited Pt surface path, whereas the gray dashed line represents the YSZ surface path with an exponential I-η relation. All values correspond to circular electrodes with 100 μm in diameter. (a) Inverse polarization resistance for equilibrium conditions. (b) Current at -0.5 V overpotential. (c) Current at -1.0 V overpotential. (d) Current at -1.5 V overpotential. (e) Current at -2.0 V overpotential. The blue cross indicates the current via the TPB, calculated from ^{18}O incorporation experiments in Ref. (13).

References

1. W. H. Nernst, *Zeitschrift für Elektrochemie*, **6**, 41 (1899).
2. J. Riegel, H. Neumann and H. M. Wiedenmann, *Solid State Ionics*, **152-153**, 783 (2002).
3. E. Ivers-Tiffée, K. H. Härdtl, W. Menesklou and J. Riegel, *Electrochim. Acta*, **47**, 807 (2001).
4. H. Huang, M. Nakamura, P. Su, R. Fasching, Y. Saito and F. B. Prinz, *J. Electrochem. Soc.*, **154**, B20 (2007).
5. A. Evans, A. Bieberle-Hutter, L. J. Bonderer, P. Chen, D. Hodel, J. L. Rupp and L. J. Gauckler, *ECS Transactions*, **25**, 989 (2009).
6. C. Falgairette and G. Fóti, *Catalysis Today*, **146**, 274 (2009).
7. J. Hertz, A. Rothschild and H. Tuller, *J. Electroceram.*, **22**, 428 (2009).
8. T. Horita, N. Sakai, H. Yokokawa, M. Dokiya and T. Kawada, *Solid State Ionics (Proceedings of the 10th International Conference on Solid State Ionics)*, **86-88**, 1259 (1996).
9. J. Janek, B. Luerßen, E. Mutoro, H. Fischer and S. Günther, *Topics in Catalysis*, **44**, 399 (2007).
10. E. Mutoro, N. Baumann and J. Janek, *The Journal of Physical Chemistry Letters*, 2322 (2010).
11. E. Mutoro, B. Luerßen, S. Günther and J. Janek, *Solid State Ionics*, **180**, 1019 (2009).
12. A. K. Opitz and J. Fleig, *Solid State Ionics*, **181**, 684 (2010).
13. A. K. Opitz, A. Schintlmeister, H. Hutter and J. Fleig, *Phys. Chem. Chem. Phys.*, **12**, 12734 (2010).
14. R. Radhakrishnan, A. V. Virkar and S. C. Singhal, *J. Electrochem. Soc.*, **152**, A927 (2005).
15. S. B. Adler, *Chem. Rev.*, **104**, 4791 (2004).
16. J. Fleig, *Annual Review of Materials Research*, **33**, 361 (2003).
17. L. Bay and T. Jacobsen, *Solid State Ionics*, **93**, 201 (1997).
18. M. W. Breiter, K. Leeb and G. Fafilek, *Journal of Electroanalytical Chemistry*, **434**, 129 (1997).
19. G. Fóti, A. Jaccoud, C. Falgairette and C. Comninellis, *J. Electroceram.*, **23**, 175 (2009).
20. J. L. Hertz and H. L. Tuller, *J. Electrochem. Soc.*, **154**, B413 (2007).
21. A. Jaccoud, C. Falgairette, G. Fóti and C. Comninellis, *Electrochim. Acta*, **52**, 7927 (2007).
22. T. Jacobsen and L. Bay, *Electrochim. Acta*, **47**, 2177 (2002).
23. Y. B. Kim, C.-M. Hsu, S. T. Connor, T. M. Gur, Y. Cui and F. B. Prinz, *J. Electrochem. Soc.*, **157**, B1269 (2010).
24. H. Kishimoto, N. Sakai, K. Yamaji, T. Horita, M. E. Brito, H. Yokokawa, K. Amezawa and Y. Uchimoto, *Solid State Ionics*, **179**, 347 (2008).
25. N. Kotsionopoulos and S. Bebelis, *Journal of Applied Electrochemistry*, **35**, 1253 (2005).
26. B. Luerßen, E. Mutoro, H. Fischer, S. Günther, R. Imbihl and J. Janek, *Angewandte Chemie International Edition*, **45**, 1473 (2006).
27. A. Mitterdorfer and L. J. Gauckler, *Solid State Ionics*, **117**, 187 (1999).
28. A. Mitterdorfer and L. J. Gauckler, *Solid State Ionics*, **120**, 211 (1999).
29. J. Mizusaki, K. Amano, S. Yamauchi and K. Fueki, *Solid State Ionics*, **22**, 313 (1987).
30. J. Mizusaki, K. Amano, S. Yamauchi and K. Fueki, *Solid State Ionics*, **22**, 323 (1987).
31. E. Mutoro, S. Günther, B. Luerßen, I. Valov and J. Janek, *Solid State Ionics*, **179**, 1835 (2008).
32. E. Mutoro, B. Luerssen, S. Günther and J. Janek, *Solid State Ionics*, **179**, 1214 (2008).
33. J. Nielsen and T. Jacobsen, *Solid State Ionics*, **178**, 1001 (2007).
34. A. K. Opitz, A. Lutz, M. Kubicek, F. Kubel, H. Hutter and J. Fleig, *Electrochim. Acta*, **56**, 9727 (2011).
35. N. L. Robertson and J. N. Michaels, *J. Electrochem. Soc.*, **137**, 129 (1990).
36. N. L. Robertson and J. N. Michaels, *J. Electrochem. Soc.*, **138**, 1494 (1991).
37. C. Schwandt and W. Weppner, *J. Electrochem. Soc.*, **144**, 3728 (1997).
38. S. N. Shkerin, *Russian Journal of Electrochemistry*, **39**, 863 (2003).
39. V. Srot, M. Watanabe, C. Scheu, P. A. van Aken, U. Salzberger, B. Luerßen, J. Janek and M. Rühle, *Solid State Ionics*, **181**, 1616 (2010).
40. V. Stancovski, S. Sridhar and U. B. Pal, *J. Electroceram.*, **3**, 279 (1999).
41. C. G. Vayenas, S. Bebelis and S. Ladas, *Nature*, **343**, 625 (1990).

42. C. G. Vayenas, S. Bebelis, V. Yentekakis, P. Tsiakaras and H. Karasali, *Platinum Metals Review*, **34**, 122 (1990).

43. M. J. Verkerk and A. J. Burggraaf, *J. Electrochem. Soc.*, **130**, 78 (1983).

44. M. J. Verkerk, M. W. J. Hammink and A. J. Burggraaf, *J. Electrochem. Soc.*, **130**, 70 (1983).

45. D. Y. Wang, *J. Electrochem. Soc.*, **137**, 3660 (1990).

46. B. Luerßen, J. Janek and R. Imbihl, *Solid State Ionics*, **141**, 701 (2001).

47. J. L. Hertz and H. L. Tuller, *Solid State Ionics*, **178**, 915 (2007).

48. T. Kawada, T. Horita, N. Sakai, H. Yokokawa, M. Dokiya and J. Mizusaki, *Solid State Ionics*, **131**, 199 (2000).

49. B. K. Lee, Y. H. Yu, B. S. So, S. M. Kim, J. Kim, H. W. Lee, J. H. Lee and J. H. Hwang, *J. Electroceram.*, **17**, 735 (2006).

50. S. P. Yoon, S. W. Nam, S.-G. Kim, S.-A. Hong and S.-H. Hyun, *Journal of Power Sources*, **115**, 27 (2003).

51. S. Koc, G. J. la O', T. Golfinopoulos and Y. Shao-Horn, *ECS Transactions*, **7**, 1271 (2007).

52. D. Y. Wang and A. S. Nowick, *J. Electrochem. Soc.*, **126**, 1166 (1979).

53. T. Kenjo, Y. Yamakoshi and K. Wada, *J. Electrochem. Soc.*, **140**, 2151 (1993).

54. B. Zachau-Christiansen, T. Jacobsen, L. Bay and S. Skaarup, *Solid State Ionics*, **113**, 271 (1998).

55. R. Schmiedl, V. Demuth, P. Lahnor, H. Godehardt, Y. Bodschwinna, C. Harder, L. Hammer, H. P. Strunk, M. Schulz and K. Heinz, *Applied Physics a-Materials Science & Processing*, **62**, 223 (1996).

56. R. Stumpf, C.-L. Liu and C. Tracy, *Applied Physics Letters*, **75**, 1389 (1999).

57. T. Ryll, H. Galinski, L. Schlagenhauf, P. Elser, J. L. M. Rupp, A. Bieberle-Hutter and L. J. Gauckler, *Advanced Functional Materials*, **21**, 565 (2011).

58. G. Beck, H. Fischer, E. Mutoro, V. Srot, K. Petrikowski, E. Tchernychova, M. Wuttig, M. Ruhle, B. Luerßen and J. Janek, *Solid State Ionics*, **178**, 327 (2007).

59. E. Ahlgren and F. Willy Poulsen, *Solid State Ionics*, **70-71**, 528 (1994).

60. J. Fleig, F. S. Baumann, V. Brichzin, H.-R. Kim, J. Jamnik, G. Cristiani, H.-U. Habermeier and J. Maier, *Fuel Cells*, **6**, 284 (2006).

61. J. Fleig, *Solid State Ionics*, **161**, 279 (2003).

62. F. S. Baumann, J. Fleig, H. U. Habermeier and J. Maier, *Solid State Ionics*, **177**, 1071 (2006).

63. C. H. Hamann and W. Vielstich, *Electrochemistry*, Wiley-VCH, Weinheim (1998).

64. J. Newman, *J. Electrochem. Soc.*, **113**, 501 (1966).

65. J. Van Herle, A. J. McEvoy and K. Ravindranathan Thampi, *Electrochim. Acta*, **39**, 1675 (1994).

66. K. V. Jensen, R. Wallenberg, I. Chorkendorff and M. Mogensen, *Solid State Ionics*, **160**, 27 (2003).

67. J. Janek and C. Korte, *Solid State Ionics*, **116**, 181 (1999).

68. J. H. Park and R. N. Blumenthal, *J. Electrochem. Soc.*, **136**, 2867 (1989).

69. J. Maier, in *Physical Chemistry of Ionic Materials - Ions and Electrons in Solids*, p. 454, John Wiley & Sons, Ltd (2004).

70. J. Fleig, *Zeitschrift Fur Physikalische Chemie-International Journal of Research in Physical Chemistry & Chemical Physics*, **221**, 1149 (2007).

71. L. Heyne and N. M. Beekman, *Proceedings of the British Ceramic Society*, **19**, 229 (1971).

72. W. C. Chueh, W. Lai and S. M. Haile, *Solid State Ionics*, **179**, 1036 (2008).

73. J. Fleig, *Phys. Chem. Chem. Phys.*, **7**, 2027 (2005).

74. M. Hendriks, J. E. ten Elshof, H. J. M. Bouwmeester and H. Verweij, *Solid State Ionics*, **146**, 211 (2002).

75. M. Hendriks, J. E. ten Elshof, H. J. M. Bouwmeester and H. Verweij, *Solid State Ionics*, **154**, 467 (2002).

76. J. R. Macdonald, in *Impedance Spectroscopy*, p. 88, John Wiley & Sons (1987).

77. J. Jamnik and J. Maier, *J. Electrochem. Soc.*, **146**, 4183 (1999).

78. J. Fleig, A. Schintlmeister, A. Opitz and H. Hutter, *Scripta Materialia*, **65**, 78 (2011).

79. R. Baker, J. Guindet and M. Kleitz, *J. Electrochem. Soc.*, **144**, 2427 (1997).